


Strong-form meshfree collocation method for multibody thermomechanical contact

Andrew Beel¹ · Jeong-Hoon Song¹ 

Received: 29 May 2021 / Accepted: 14 September 2021 / Published online: 28 October 2021
© The Author(s), under exclusive licence to Springer-Verlag London Ltd., part of Springer Nature 2021

Abstract

This study presents a strong form-based meshfree point collocation method for thermomechanical contact between two deformable bodies. The proposed method, based on Taylor approximation and the method of moving least squares, is implemented in a staggered Newton–Raphson framework to directly discretize and solve the governing nonlinear system of partial differential equations. Following the formulation of the proposed method and the discretization of the governing equations, four numerical examples are presented to verify the computational framework described. The first two examples, involving frictional contact along an inclined surface and Hertzian contact between two half-cylinders, verify the method’s ability to simulate two-body mechanical contact. The next two examples, involving coupled mechanical and thermal contact between rectangular blocks for two loading conditions, verify the ability of the method to simulate thermomechanical contact.

Keywords Multibody contact · Thermo-mechanical interaction · Strong form · Meshfree · Collocation

1 Introduction

The mechanics of contact, particularly thermomechanical contact, has wide-ranging applications in engineering, from modeling automobile crash safety to hip joint replacements to pellet-cladding interactions in a nuclear fuel rod [1–3]. Due to the nonlinear dependence of the contact traction and heat flux on the displacement and temperature fields, the governing equations for thermomechanical contact are nonlinear. In many of the applications of thermomechanical contact, coupling between the mechanical and thermal fields is an important concern. For example, temperature changes may cause significant thermal expansion, mechanical friction may generate significant heat, and degree of heat transfer across contact surfaces may depend significantly on the contact pressure [1, 4]. These applications and concerns have motivated the development of computational methods for solving contact problems numerically.

In the majority of computational studies of contact problems, the numerical methods are often required because of sharp gradients observed near transitions between stick and slip conditions and near the edges of

By directly discretizing the strong form of governing PDEs using a set of approximate derivative operators, the proposed method avoids mesh dependency, domain integration, and exact computation of derivatives [14]. In addition, the proposed method easily treats boundary conditions and adaptive

where \mathbf{e}_3 is the unit basis vector pointing out of the paper. It is convenient to decompose the contact traction \mathbf{t}^c at a point \mathbf{x} into components along $\boldsymbol{\nu}$ and $\boldsymbol{\tau}$, as follows:

The length of \mathbf{p} and \mathbf{a} is $L_p = \frac{(n_{\text{dim}}+m)!}{n_{\text{dim}}!m!}$. The integer arrays $\alpha_1, \dots, \alpha_{L_p}$ are in lexicographical order by convention.

Now, consider a set of N collocation points on a domain Ω . If the value of u is known only at each of these N points, the vector \mathbf{u} of derivative coefficients must be found approximately. The best vector \mathbf{u}^* in the weighted least squares sense is found by minimizing the functional

Here, w is a weight function with a compact support, i.e., positive inside and zero outside of a closed disk of radius $\rho(\mathbf{x})$ surrounding $\bar{\mathbf{x}}$. The radius ρ , called the dilation parameter, may vary with the location of the local center over the domain Ω to adjust for spatial variation in the density and pattern of collocation points. Differentiating \mathcal{F} with respect to \mathbf{u} and setting the result equal to zero yields the optimal approximate derivative coefficient vector \mathbf{u}^* , given by

Here, the matrix \mathbf{M} is given by

The matrix \mathbf{B} is given by

Note that the weight function w is not differentiated in this formulation, so non-smooth weight functions may be used.

For a single local center $\bar{\mathbf{x}}$, the approximate derivative vector \mathbf{u}^* minimizes the weighted least square residual globally. However, a best local approximation at each collocation point may be found by moving the local center to each collocation point \mathbf{x} , hence the term “moving least squares.” Thus, taking $\bar{\mathbf{x}} \rightarrow \mathbf{x}$, the best \mathbf{u}^* in the moving least squares sense at each collocation point \mathbf{x} is given by

Since the α^{th} entry of $\mathbf{a}(\mathbf{x})$ is an approximation for the α^{th} derivative of u evaluated at \mathbf{x} , the corresponding row of

(

The second solution vector is the nodal temperature change vector, given by

Here, \mathbf{x} is the i th collocation point, N is the total number of collocation points, u_i^h corresponds to the i th displacement degree of freedom, and T^h corresponds to the temperature change. In the present study, there are a total of three degrees of freedom, namely the x - and y -components

The strong form of the PDEs in (4.4) are discretized by replacing the various derivative terms with approximate derivatives constructed using the differential operators from Chapter 3. This discretization is used to construct the equations for each interior collocation point. Suppose $\mathbf{x} \in \Omega$ is an interior collocation point and let Φ_{IJ}^α represent the J th entry of the α^{th} differential operator at collocation point \mathbf{x} . Then, the equations in (4.4) for node $\mathbf{x} \in \Omega$ are discretized as

Thus, for node $\mathbf{x} \in \Omega$, the 2×2 IJ block of \mathbf{K}_U is given by the partial derivative of (4.5) with respect to $\{u_1^h(\mathbf{x}_J), u_2^h(\mathbf{x}$

displacement and strain assumption. The nonlinearity for the contact problem in this study comes solely from the contact constraints, discretized in the following section.

4.2 Discretization of regularized mechanical contact constraints

Like the traction boundary condition (2.7)₂, the contact condition (2.7)₃ contains the σ term. Unlike prescribed traction $\bar{\mathbf{t}}$, however, the contact traction \mathbf{t}^c depends on the displacement field. To discretize the contact constraints, we begin by substituting (2.10) in (2.7)₃ and writing this equation in index notation:

The values of contact pressure t_N and tangential traction t_T depend on the gap function and the slip/stick state of the system, as explained in Sect. 2. The gap function is discretized

above are simply concatenated $I = 1 : N$ according to the type (interior, boundary, contact, etc.) of node I . Thus, the I^{th} block of \mathbf{R}_U , i.e., entries $2I - 1$ and $2I$ of \mathbf{R}_U , is given by

Similarly, the IJ block of \mathbf{K}_U is given by

Note that the tangent stiffness matrix \mathbf{K}_U

the stress field, the contact algorithm, and an ABAQUS FEM model. The FEM model was chosen to have roughly the

near the edge of the contact boundary. However, as the collocation point arrangement is further refined, the discrepancy between the computed and analytical solution near the edge of the contact boundary is reduced. It should also be noted that finite-element methods such as [9] experience

5.3 Thermomechanical contact between rectangular blocks

problem for various values of prescribed displacement. Figure 17 shows contour plots of the components of displacement and temperature for $\bar{u}_y = -1.0 \times 10^{-3}$. The computed displacement and temperature fields in Fig. 17 are reasonable. As expected in the x -displacement field, the top and bottom edges are held fixed in the x -direction while the left and right sides experience a Poisson's effect. The y -component of displacement has an approximately constant slope in the y -direction, as expected since the two blocks have the same material properties. Any discrepancy from constant strain ϵ_{yy} can be explained by the thermal expansion of the top block. Finally, the temperature field has a jump at the contact interface but there is a temperature gradient across each block, reflecting the imperfect, i.e., *flux-resistant* heat conduction across the interface modeled by Eq. (2.22).

Beyond these initial assurances, the numerical solution is verified by its agreement with the analytical solution for the temperature jump across the contact interface. The analytical temperatures along the contact interface are computed based on the computed contact pressure because an analytical solution based directly on prescribed displacement is unavailable. Figure 18 shows that the temperature jump across the contact interface becomes smaller as the contact pressure increases because the increased contact pressure makes the surface more conductive, as expected.

It also shows that the analytical temperature vs. contact pressure is visually indistinguishable from the computed solution. The maximum relative error between the analytical temperature and the computed temperature is

$$\frac{\max_{\text{exact}} - \max_{\text{numer}}}{\max_{\text{exact}}} = 2.3 \times 10^{-4}. \quad (5.4)$$

The numerical results from this section verify the implementation of the proposed method for thermomechanical contact. From the first example, it is clear that the method

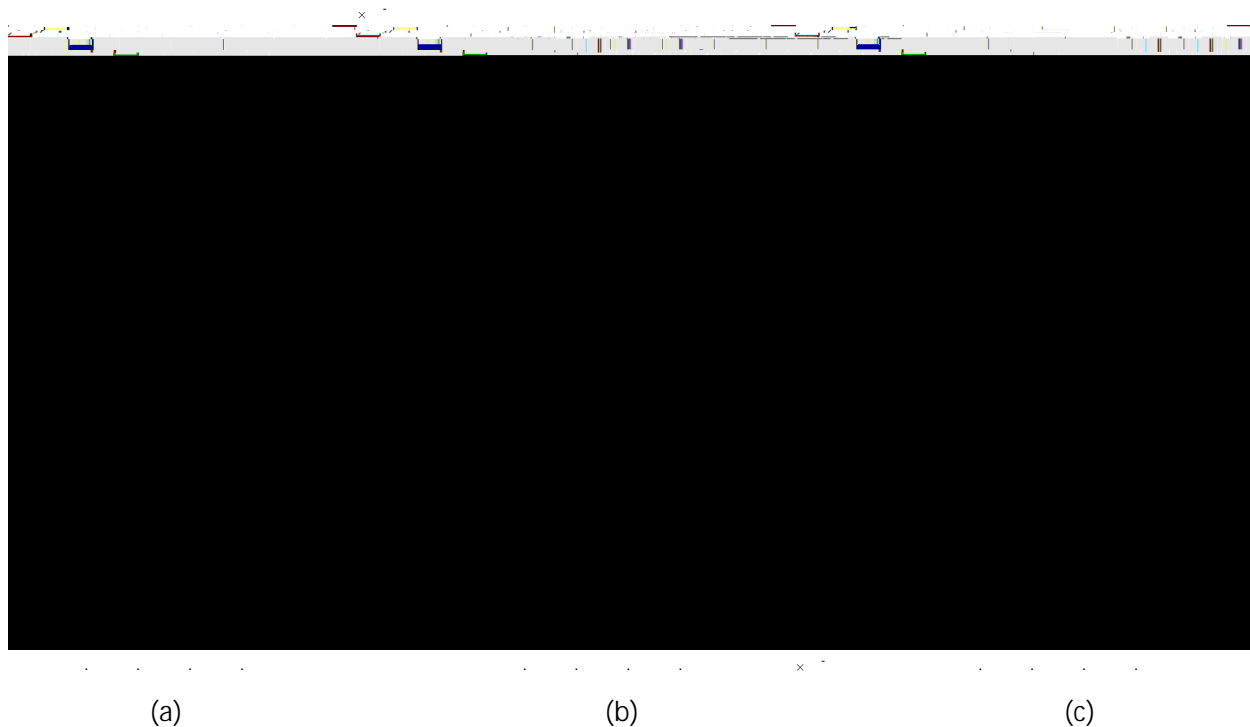


Fig. 17 **a** x -component of displacement, **b** y

can accurately distinguish between stick and slip in the case of frictional contact. The second example (Hertzian contact) demonstrates that the proposed method can successfully match the analytical solution for a nontrivial contact pressure profile in the frictionless case and predict a reliable numerical solution of the governing equations in the frictional case. Based on the third example, the method can handle the additional nonlinearity of the thermal field, since the

27. Song JH, Fu Y, Kim TY, Yoon YC, Michopoulos JG, Rabczuk T (2018) Phase field simulations of coupled microstructure solidification problems via the strong form particle difference method. *Int J Mech Mater Des* 14:491–509
28. Fu Y, Michopoulos JG, Song JH (2017) Bridging the multi phase-field and molecular dynamics models for the solidification of nano-crystals. *J Comput Sci* 20:187–197
29. Almasi A, Beel A, Kim T-Y, Michopoulos JG, Song J-H (2019) Strong-form collocation method for solidification and mechanical analysis of polycrystalline materials. *J Eng Mech* 145(10):04019082
30. Yoon YC, Schaeferkoetter P, Rabczuk T, Song JH (2019) New strong formulation for material nonlinear problems based on the particle difference method. *Eng Anal Boundary Elem* 98:310–327
31. Almasi A, Kim T-Y, Laursen TA, Song J-H (2019) A strong form meshfree collocation method for frictional contact on a rigid obstacle. *Comput Methods Appl Mech Eng* 357:112597
32. Beel A, Kim TY, Jiang W, Song JH (2019) Strong form-based meshfree collocation method for wind-driven ocean circulation. *Comput Methods Appl Mech Eng* 351:404–421
33. Aluru NR (2000) A point collocation method based on reproducing kernel approximations. *Int J Numer Meth Eng* 47:1083–1121
34. Hu HY, Chen JS, Hu W (2011) Error analysis of collocation method based on reproducing kernel approximation. *Numer Methods Part Differ Equ* 27:554–580
35. De Lorenzis L, Evans JA, Hughes TJR, Reali A (2015) Isogeometric collocation: Neumann boundary conditions and contact. *Comput Methods Appl Mech Eng* 284:21–54
36. Kruse R, Nguyen-Thanh N, De Lorenzis L, Hughes TJR (2015) Isogeometric collocation for large deformation elasticity and frictional contact problems. *Comput Methods Appl Mech Eng* 296:73–112
37. Yeung S-K, Weeger O, Dunn ML (2017) Isogeometric collocation methods for Cosserat rods and rod structures. *Comput Methods Appl Mech Eng* 316:100–122
38. Novascone SR, Spencer BW, Hales JD, Williamson RL (2015) Evaluation of coupling approaches for thermomechanical simulations. *Nucl Eng Des* 295:910–921